J Biomol NMR (2015) 61:123–136
DOI 10.1007/s10858-014-9894-3

ARTICLE

A minor conformation of a lanthanide tag on adenylate kinase characterized by paramagnetic relaxation dispersion NMR spectroscopy

Mathias A. S. Hass · Wei-Min Liu · Roman V. Agafonov · Renee Otten · Lien A. Phung · Jesika T. Schilder · Dorothee Kern · Marcellus Ubbink

Received: 30 October 2014 / Accepted: 22 December 2014 / Published online: 8 January 2015

Abstract NMR relaxation dispersion techniques provide a powerful method to study protein dynamics by characterizing lowly populated conformations that are in dynamic exchange with the major state. Paramagnetic NMR is a versatile tool for investigating the structures and dynamics of proteins. These two techniques were combined here to measure accurate and precise pseudocontact shifts of a lowly populated conformation. This method delivers valuable long-range structural restraints for higher energy conformations of macromolecules in solution. Another advantage of combining pseudocontact shifts with relaxation dispersion is the increase in the amplitude of dispersion profiles. Lowly populated states are often involved in functional processes, such as enzyme catalysis, signaling, and protein/protein interactions. The presented results also unveil a critical problem with the lanthanide tag used to generate paramagnetic relaxation dispersion effects in proteins, namely that the motions of the tag can interfere severely with the observation of protein dynamics. The two-point attached CLaNP-5 lanthanide tag was linked to adenylate kinase. From the paramagnetic relaxation dispersion only motion of the tag is observed. The data can be described accurately by a two-state model in which the protein-attached tag undergoes a 23° tilting motion on a timescale of milliseconds. The work demonstrates the large potential of paramagnetic relaxation dispersion and the challenge to improve current tags to minimize relaxation dispersion from tag movements.

Keywords Relaxation dispersion · Lanthanide binding tags · Protein dynamics · Paramagnetic NMR · Caged lanthanide NMR probe · Adenylate kinase

Introduction

The structure and dynamics of proteins form the basis of biomolecular function. Traditionally, structure and dynamics have been studied separately, presumably for practical experimental reasons: To determine a structure and simultaneously see it move is challenging indeed, although good progress has been made in considering nanosecond dynamics (Torda et al. 1990; Cornilescu et al. 1998; Bouvignies et al. 2006; Markwick et al. 2009). A major step forward in characterizing dynamics has been the development of new NMR methods, in particular relaxation dispersion techniques (Palmer et al. 2001). These techniques have provided experimental support for the idea that the ground state of proteins coexists in a dynamic equilibrium with other conformations, whose energies are only slightly higher than that of the ground state. Several studies have suggested that these alternative conformations are likely to be functional, e.g. in enzyme catalysis (Vallurupalli et al. 2007; Wang et al. 2007; Vallurupalli et al. 2008a, b; Bouvignies et al. 2011). This idea echoes the well-known concept of allostery, most prominently featured in the Monod–Wyman–Changeux model (Monod et al. 1965). Experimental verification of such models is

Electronic supplementary material The online version of this article (doi:10.1007/s10858-014-9894-3) contains supplementary material, which is available to authorized users.

M. A. S. Hass · W.-M. Liu · J. T. Schilder · M. Ubbink (✉)
Leiden Institute of Chemistry, Leiden University, Einsteinweg 55, 2333 CC Leiden, The Netherlands
e-mail: m.ubbink@chem.leidenuniv.nl

R. V. Agafonov · R. Otten · L. A. Phung · D. Kern
Department of Biochemistry, Howard Hughes Medical Institute, Brandeis University, 415 South Street, Waltham, MA 02454, USA

notoriously difficult because it requires structural characterization of lowly populated protein states that are in dynamic exchange with the ground state. These higher energy states are often not directly observable in the NMR spectrum. Yet, they may manifest themselves through line broadening of the NMR signals, an effect commonly known as chemical exchange. Chemical exchange in proteins can be monitored by NMR relaxation dispersion, whereby information about the exchanging states is acquired. Conventional relaxation dispersion studies can determine the chemical shifts of lowly populated states (Palmer et al. 2001) and more recently, relaxation dispersion experiments have been designed for measuring residual dipolar couplings (RDC) (Vallurupalli et al. 2007, 2008b) and residual anisotropic chemical shifts (RACS) (John et al. 2005; Vallurupalli et al. 2008a) of these states. Despite these advances, it remains challenging to obtain sufficient information on these minor states to allow their structures to be determined. Although chemical shifts can be related to the protein structure (Bouvignies et al. 2011), RDCs and RACSs provide more accurate structural information, but exquisite data quality is essential to measure these relatively small NMR effects (Vallurupalli et al. 2007; Vallurupalli et al. 2008b)—a quality often not feasible to obtain.

An alternative method that has been proposed recently, is to use the relaxation dispersion technique to measure pseudocontact shifts (PCS) (Wang et al. 2007; Eichmueller and Skrynnikov 2007; Hass et al. 2010). Most importantly, this method promises powerful long-range restraints for structure determination of minor protein conformations. To achieve this, a paramagnetic ion is used to create a PCS gradient throughout the protein (Fig. 1c), causing any nucleus that moves relative to the paramagnet to experience a fluctuation in its resonance frequency and thereby inducing relaxation dispersion (Wang et al. 2007; Eichmueller and Skrynnikov 2007; Hass et al. 2010).

Besides providing long-range structural restraints, the paramagnetic approach has several other advantages. Large dispersion effects can be achieved for more nuclei than with RDCs, RCSAs, or even diamagnetic chemical shifts. Furthermore, the paramagnetic effects can be tuned by the choice of paramagnet. In this way the relaxation dispersion effect can be varied and controlled in a manner that is not possible in conventional diamagnetic experiments. This novel paramagnetic method requires the incorporation of a paramagnetic center with an anisotropic magnetic susceptibility. An elegant way to achieve this is to use natural metal binding sites that can accommodate a lanthanide (Ln) ion, such as Ca^{2+}-binding sites (Wang et al. 2007; Eichmueller and Skrynnikov 2007). A more general approach is to use Ln-binding tags that can be attached to any protein (Eichmueller and Skrynnikov 2007; Hass et al. 2010). Yet, the tag must be dynamically restricted to avoid extensive averaging of the anisotropic paramagnetic effect. Thus, an attempt to use a highly flexible EDTA-based Ln tag to observe paramagnetic relaxation dispersion was reported to be unsuccessful because the PCS were too small and a low signal-to-noise ratio of the resonances was obtained due to motions of the tag (Eichmueller and Skrynnikov 2007). More recently, two-point attached lanthanide binding tags have been developed (Fig. 1a) (Otting 2008; Keizers and Ubbink 2011; Koehler and Meiler 2011), and it has been shown that large paramagnetically induced relaxation dispersion effects can be observed when the Ln tag is conformationally restricted in this way (Hass et al. 2010). However, so far paramagnetic relaxation dispersion effects have only been interpreted qualitatively (Wang et al. 2007; Eichmueller and Skrynnikov 2007; Hass et al. 2010). To investigate dynamics by paramagnetic relaxation dispersion in a quantitative way the two-armed Ln tag CLaNP-5 (Keizers et al. 2007, 2008) was attached to adenylate kinase (ADK) from *Aquifex aeolicus* (*A.a.*).

This tag has been shown to be dynamically restricted as well as tightly bound to its lanthanide ion (Keizers et al. 2008). Although the two-point attachment reduces the amplitude of the tag mobility, motions can still occur. If these motions occur on the μs–ms time-scale, where relaxation dispersion experiments are sensitive, they cause relaxation dispersion, which may interfere with the observation of protein dynamics. Previously, it was observed that movements of the CLaNP-5 tag in some cases induced large paramagnetic relaxation dispersion, even when attached to a rigid protein (Hass et al. 2010). In the current study, we chose to attach the tag to two cysteines introduced at positions separated by one helical turn in a well-defined α-helix of ADK (Fig. 1a), with the aim to minimize tag movements relative to the protein.

ADK is an enzyme known for undergoing major structural changes during its catalytic cycle (Wolf-Watz et al. 2004; Henzler-Wildman et al. 2007a). The rate-limiting step in the catalytic cycle is a large-scale lid-opening and closing. Previous studies have shown that similar lid-opening and closing occurs in the absence of substrates. These dynamics were very difficult to detect due to the small amplitude of the dispersion curves, and in fact, remained undetected at room temperature (Henzler-Wildman et al. 2007a). Our relaxation dispersion studies on the paramagnetically tagged protein show extensive dispersion effects throughout the protein, even at 318 K. However, a detailed analysis shows that the relaxation dispersion of this Ln-tagged ADK molecule is not caused by the movement of the protein but primarily by a subtle tilting motion of the lanthanide tag. So, conformational exchange characterized in this study is not directly relevant for understanding ADK, yet it proves to be a useful model

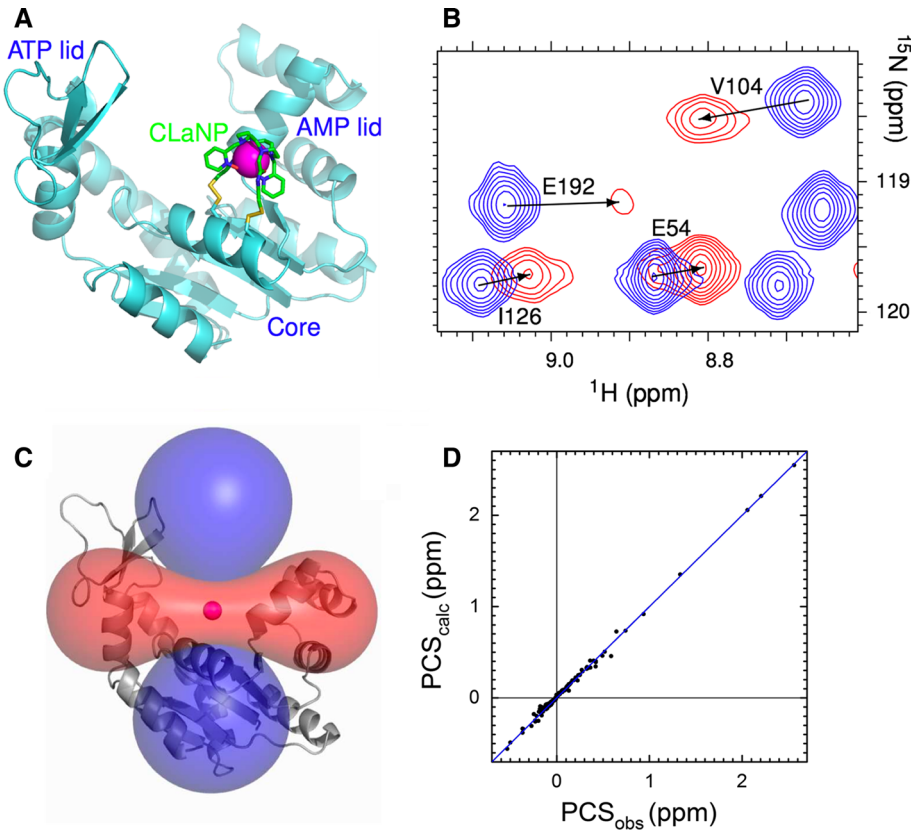

Fig. 1 **a** The CLaNP-5 tag and two mutations (K18C/K22C), shown in *stick* representation, were modeled on the structure of *A.a.* ADK (pdb id: 2RH5) (Henzler-Wildman et al. 2007a) shown as ribbons. The lanthanide is shown by a *pink sphere*. **b** Detail of the ^{15}N HSQC spectrum of diamagnetic Lu-labeled ADK(K18C/K22C) (*blue*) and paramagnetic Yb-labeled ADK (*red*). **c** The PCS isosurface of Yb^{3+} with a PCS of −0.15 ppm (*red*) and +0.15 ppm (*blue*). **d** Calculated versus observed PCSs. The PCSs were calculated on the basis the crystal structure of ADK and averaged for chains A–C, and the Δχ-tensor and lanthanide position fitted to the observed PCS

system that mimics domain motions in proteins. This work outlines a procedure for obtaining PCSs of a lowly populated conformation from relaxation dispersion experiments and uses them to characterize that state structurally. Importantly, the PCSs measured indirectly by relaxation dispersion were validated by direct observation of the minor state at a low temperature, where its NMR signals are visible in the spectrum. The relaxation dispersion derived PCSs are shown to be accurate and precise, suitable for atomic resolution structure calculations. These results show how promising paramagnetic relaxation dispersion is for characterizing lowly populated states structurally, providing an impetus for further development of Ln tags to overcome current problems associated with tag motions.

Theory

A paramagnetic ion with an anisotropic magnetic susceptibility gives rise to a PCS for surrounding nuclei, given by (Bertini et al. 2002):

$$\mathrm{PCS} = \frac{1}{12\pi r^3}\left[\Delta\chi_{\mathrm{ax}}\left(3\cos^2\theta - 1\right) + \frac{3}{2}\Delta\chi_{\mathrm{rh}}\left(\sin^2\theta\cos 2\phi\right)\right] \quad (1)$$

The distance r and the angles θ, and φ are the spherical coordinates of the nucleus with respect to the frame of the magnetic susceptibility tensor (χ) with its origin at the paramagnetic center. The anisotropy of the χ-tensor, Δχ, is described by an axial and rhombic component, $\Delta\chi_{\mathrm{ax}}$ and $\Delta\chi_{\mathrm{rh}}$, respectively. The PCS is temperature dependent and follows approximately Curie's law (Bertini et al. 2002), according to which the magnetization (here manifested in the form of the PCS) is inversely proportional to the temperature.

Experimental PCSs are measured as the difference between the chemical shifts in the paramagnetic molecule (δ_{para}) and the corresponding shifts in a suitable diamagnetic analog (δ_{dia}), thus, $\mathrm{PCS} = \delta_{\mathrm{para}} - \delta_{\mathrm{dia}}$. This is an approximation since in certain cases other paramagnetic effects also can affect the shift significantly (Bertini et al. 2002; Koehler and Meiler 2011).

Anisotropic paramagnets cause partial alignment that induces RDC and RACS (John et al. 2005). For a paramagnet attached rigidly to a molecule, the alignment is proportional to Δχ and it increases with the square of the magnetic field.

Paramagnetic relaxation enhancement (PRE) causes signals from nuclei close to the paramagnet to broaden. For lanthanides (used in this work) the PRE is dominated by Curie-spin relaxation, which is nearly proportional to the rotational correlation time of the protein and proportional to r^{-6} (Koehler and Meiler 2011). Still, since the PCS is proportional to r^{-3} (Eq. 1), the PCS can be observed far beyond the range where PRE causes severe line broadening.

To analyze chemical exchange effects in the presence of an anisotropic paramagnet a simple two-site exchange between two conformational states A and B is considered:

$$\mathrm{A} \underset{k_B}{\overset{k_A}{\rightleftarrows}} \mathrm{B} \tag{2}$$

The exchange rate is the sum of the two rate constants, $k_{ex} = k_A + k_B$, and the populations of the two states, p_A and p_B, are related by $p_A = (1 - p_B)$. Here it is assumed that $p_B \leq p_A$. A given nucleus has a resonance frequency of ω_A and ω_B in state A and B, respectively. The difference in the resonance frequency is defined as $\Delta\omega = \omega_B - \omega_A$. The line-broadening effect from chemical exchange is given by the three parameters k_{ex}, p_B, and $\Delta\omega$. The process is in slow exchange when $k_{ex} << \Delta\omega/\sqrt{2}$ and the two states give rise to separate signals. Coalescence of the signals occurs when $k_{ex} = \Delta\omega/\sqrt{2}$, at which point the exchange broadening is at its maximum. The exchange regime close to coalescence ($k_{ex} \approx \Delta\omega/\sqrt{2}$) is referred to as intermediate exchange. When $k_{ex} >> \Delta\omega/\sqrt{2}$ the process is in the fast-exchange regime and the observed signal is a population weighted average at a frequency:

$$\omega_{obs} = p_A\omega_A + p_B\omega_B \tag{3}$$

The relaxation dispersion effect in a Carr–Purcell–Meiboom–Gill (CPMG) based experiment is the modulation of the effective transverse relaxation rate ($R_{2,eff}$) by the CPMG pulsing frequency, $\nu_{cpmg} = 1/(2\tau_{cpmg})$, where τ_{cpmg} is the time between the center of two successive π-pulses in the applied CPMG pulse train.

$$R_{2,eff} = R_2^0 + R_{ex}\left(\nu_{cpmg}\right) \tag{4}$$

R_2^0 is the effective R_2 relaxation rate in the absence of chemical exchange. R_{ex} as a function of ν_{cpmg} can be expressed by the Carver-Richards equation (Carver and Richards 1972), and depends on k_{ex}, p_B, and $|\Delta\omega|$. The CPMG dispersion does not report the sign of $\Delta\omega$.

In our notation, $\Delta\omega$ has the units rad/s; however, it is often convenient to convert this value into chemical shifts units (ppm). The $\Delta\omega$ values of the diamagnetic and paramagnetic protein in units of ppm are referred to as $\Delta\delta_{dia}$ and $\Delta\delta_{para}$, respectively.

For the diamagnetic protein, $|\Delta\omega|$ is directly related to the absolute value of the chemical shift difference $|\Delta\delta_{dia}| = |\Delta\omega|/|\omega_0|$, where ω_0 is the Larmor frequency.

In the presence of an anisotropic paramagnet there are more contributions to $\Delta\omega$:

$$\left|\Delta\delta_{para}\right| = \left|\Delta PCS + \Delta\delta_{dia} + \Delta RCSA \pm \frac{\Delta RDC}{2\omega_0}\right| \tag{5}$$

The most prominent paramagnetic contribution is ΔPCS. The contributions ΔRACS and ΔRDC that result from paramagnetic alignment are usually much smaller. ΔRACS is the difference in the residual anisotropic chemical shift between the two states. ΔRDC is the corresponding difference in the H–N residual dipolar coupling, which only contributes in spin-state-selective NMR experiments, e.g. TROSY. The sign of this contribution depends on what spin state is observed (Vallurupalli et al. 2007). The ΔRACS and ΔRDC contributions from paramagnetic alignment by Yb^{3+} are small for ^1H, which is the nucleus used in this study. The maximum RACS and RDC are expected to be about 1 and 8 ppb at 14.1 T, respectively. Therefore, these contributions are here treated as negligible:

$$\left|\Delta\delta_{para}\right| \approx \left|\Delta PCS + \Delta\delta_{dia}\right| \tag{6}$$

It follows from Eq. 6 that there are four sets of PCS values that satisfy the relaxation dispersion data for a given nucleus. In the fast-exchange regime these are:

$$\begin{aligned}
&\text{(I)} \quad PCS_A = PCS_{obs} + p_B\left(\left|\Delta\delta_{para}\right| + \left|\Delta\delta_{dia}\right|\right);\\
&\qquad PCS_B = PCS_A - \left|\Delta\delta_{para}\right| - \left|\Delta\delta_{dia}\right|\\
&\text{(II)} \quad PCS_A = PCS_{obs} - p_B\left(\left|\Delta\delta_{para}\right| - \left|\Delta\delta_{dia}\right|\right);\\
&\qquad PCS_B = PCS_A + \left|\Delta\delta_{para}\right| - \left|\Delta\delta_{dia}\right|\\
&\text{(III)} \quad PCS_A = PCS_{obs} + p_B\left(\left|\Delta\delta_{para}\right| - \left|\Delta\delta_{dia}\right|\right);\\
&\qquad PCS_B = PCS_A - \left|\Delta\delta_{para}\right| + \left|\Delta\delta_{dia}\right|\\
&\text{(IV)} \quad PCS_A = PCS_{obs} - p_B\left(\left|\Delta\delta_{para}\right| + \left|\Delta\delta_{dia}\right|\right);\\
&\qquad PCS_B = PCS_A + \left|\Delta\delta_{para}\right| + \left|\Delta\delta_{dia}\right|
\end{aligned} \tag{7}$$

where PCS_{obs} is the PCS directly observed in the spectrum (Eq. 3). If $\Delta\delta_{dia} = 0$, solutions *I* and *III* are identical, and so are *II* and *IV*. Outside the fast exchange regime the equations for PCS_A (Eqs. 7) are not exact. For instance, in the slow-exchange regime $PCS_A = PCS_{obs}$.

Experimental section

Sample preparation

The double-cysteine mutant of ADK was engineered using the QuikChange kit (Stratagene) starting from the optimized ADK gene (GenScript USA Inc.) and subcloned into vector pET-3a (Novagen). *Escherichia coli* BL21(DE3) cells were used to express the gene. Cultures were incubated to an OD_{600} of ~0.8 and induced with 0.5 mM IPTG for 6 h at 37 °C. U-[^{15}N]- and U-[^{2}H,^{15}N]-labeled proteins were produced in M9 minimal medium prepared using H_2O or D_2O, respectively. In both cases, the M9 medium contained 1 g/L $^{15}NH_4Cl$ (Cambridge Isotope Laboratories) as the sole nitrogen source and 3 g/L unlabeled D-glucose. Protein was purified using a combination of affinity, anion exchange, and size-exclusion chromatography. Purity of the protein was confirmed with gel electrophoresis. After

purification, the protein was concentrated to 100 μM in a buffer containing 50 mM Tris–HCl, 80 mM KCl, 1 mM TCEP (pH 8.0), flash-frozen in liquid nitrogen and stored at −80 °C.

The CLaNP-5-Ln tag was synthesized as previously described (Keizers et al. 2008) and attached to the protein using a procedure similar to that previously reported (Keizers et al. 2008). Dithiotreitol (5 mM) was added to a 100 μM solution of ADK(K18C/K22C) in 20 mM sodium phosphate pH 7.0 and incubated on ice for 1 h to reduce the cysteines. Excess of dithiotreitol was removed on a PD10 column (GE Healthcare) and 10 equivalents of CLaNP-5-Ln were added and stirred for 1 h on ice and centrifuged to remove precipitate. Excess of tag was removed by buffer exchange to 20 mM sodium phosphate, pH 7.0, and the protein was concentrated to 0.5 mM using a 10 K centrifugal filter (Amicon). Except for the presence of 5 % untagged protein no impurities were observed in the NMR spectrum, therefore no further purification was needed. 5 % D_2O was added for lock in the NMR samples.

NMR spectroscopy

NMR experiments were carried out on a 600 MHz Bruker Avance III spectrometer equipped with a TCI-cryo-probe. Directly observed PCS of the ground state were measured using ^{15}N HSQC spectra at 298–318 K on [^{15}N] ADK(K18C/K22C) tagged with CLaNP-5-Lu/Yb. CPMG relaxation dispersion experiments were carried out at 298, 308, and 318 K on [^{2}H, ^{15}N] ADK(K18C/K22C) tagged with CLaNP-5-Lu/Yb. The TROSY-based ^{1}H CPMG dispersion pulse sequence was a modified version of a previously published multi-quantum TROSY sequence with a CPMG element implemented just before acquisition (Orekhov et al. 2004), where the preceding TROSY sequence was replaced by a single-quantum version (Pervushin et al. 1997) to minimize loss due to chemical exchange relaxation of the protons during t_1. The constant-time CPMG delay, T_{cpmg}, was set to 40 ms and a multiple of four π-pulses with alternating phases (x, y, x, y) were applied. ^{15}N-TROSY spectra were used to directly observe PCS of both states at 278 K in [^{2}H, ^{15}N] ADK(K18C/K22C) tagged with CLaNP-5-Lu/Yb.

Data analysis

Spectra were processed with nmrPipe (Delaglio et al. 1995), and analyzed in Sparky (T. D. Goddard & D. G. Kneller, University of California, San Francisco) and CCPN analysis (Vranken et al. 2005). Intensities, $I(\nu_{cpmg})$, in the CPMG dispersion spectra were measured as the peak volume of the peaks fitted to Gauss–Lorentzian line shape using FuDA (D. F. Hansen, University College, London). The effective R_2 rate was calculated as $R_{2,eff} = \ln[I_0/I(\nu_{cpmg})]/T_{cpmg}$, where I_0 is the intensity in a reference spectrum with $T_{cpmg} = 0$. Fitting of the CPMG dispersion curves (Eq. 4) was carried out in gnuplot version 4.4. Initially, residues with significant dispersion were fitted individually in a three parameter fit, where k_{ex}, $|\Delta\omega|$, and R_2^0 were optimized assuming that $p_B = 0.2$. For residues with no significant dispersion only R_2^0 was optimized setting $|\Delta\omega| = 0$. Subsequently all residues with significant dispersion and recorded at the same temperature were used in a global fit, assuming a single two-site exchange process. Parameters k_{ex} and p_B were globally optimized for the data at 308 K using a grid search, where k_{ex} was varied between 600–800 s^{-1} and p_B 0.05–0.5. The obtained value of p_B is not precise, because most resonances are in fast exchange. In this scenario, fitting of the relaxation dispersion profiles will yield only the rate of interconversion (k_{ex}) and the product ϕ_{ex} ($p_A p_B \Delta\omega^2$) (Palmer et al. 2001). Separating this product is only possible when either of the variables (i.e., population or chemical shift difference) is known from independent measurements. A few resonances, however, are in intermediate exchange (e.g. Phe 5, Fig. 2) and their profiles provide, in principle, sufficient information to determine p_B and $\Delta\omega^2$ separately. However, due to the large R_2 rates at low ν_{cpmg} frequencies associated with intermediate exchange, these resonances give rise to weak signals and, therefore, the data quality is insufficient to determine p_B precisely. The best global fit was obtained for a population of 0.2, but other values of p_B in the range 0.1–0.5 give similar fits. A value of p_B less than 0.1 is inconsistent with the dispersion profiles as it results in significantly worse fits (Figure S1). The problem of determining the population reliably is not particular for paramagnetic systems and can in principle be addressed by acquiring relaxation dispersion data at more than one field strength, but only if the exchange process is on the intermediate timescale. However, such experiments were not undertaken in the present study. Numbat (Schmitz et al. 2008) was used to fit the $\Delta\chi$-tensors and Ln-positions. The structures used for these calculations are the three structures in the unit-cell of w.t. *A.a.* ADK crystals (PDB id. 2RH5) (Henzler-Wildman et al. 2007a). The three structures were aligned with respect to the C^α atoms in the α-helix (residues 13–24) to which CLaNP-5 is attached. Q-values were calculated according to (Cornilescu et al. 1998).

Results and discussion

Assignment of Ln-tagged ADK

ADK(K18C/K22C) was tagged with a labeling efficiency of about 95 % as judged from the intensity ratio between Yb-tagged and untagged protein signals in the ^{15}N HSQC spectrum. Spectra of Ln-tagged ADK were assigned on the

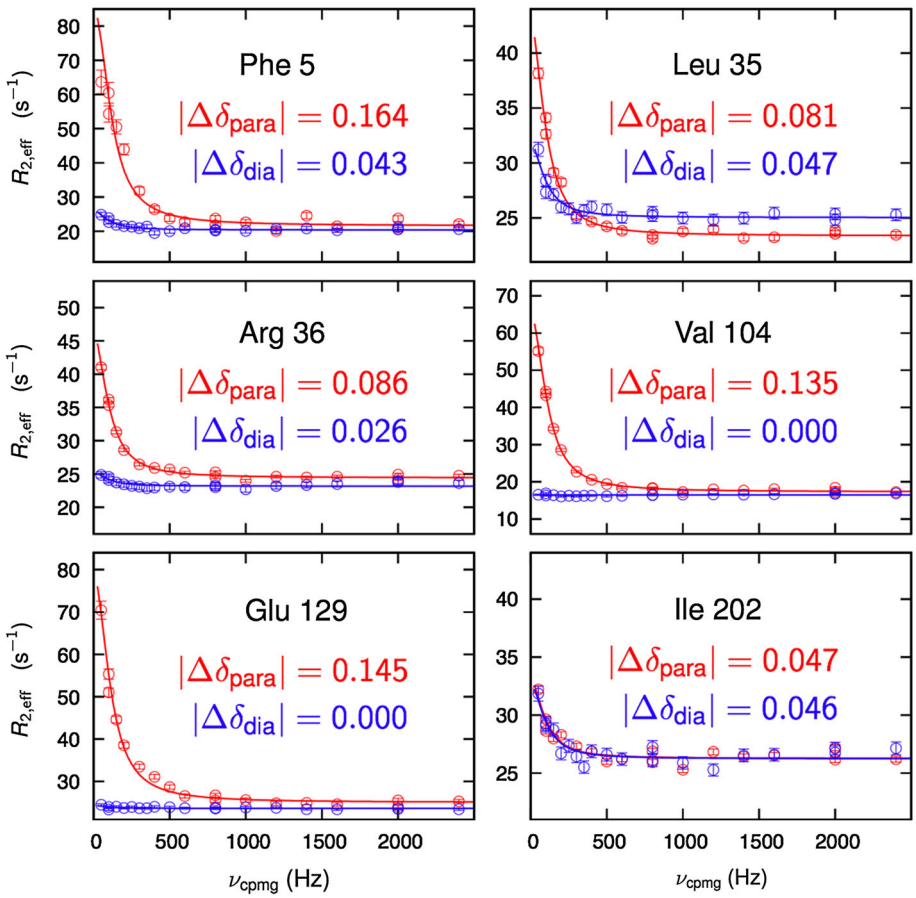

Fig. 2 Examples of amide ^{1}H CPMG dispersion profiles of ADK(K18C/K22C) tagged with CLaNP-5 loaded with Lu^{3+} (diamagnetic, *blue*) or Yb^{3+} (paramagnetic, *red*) at 308 K and 14.1 T on 0.5 mM [^{15}N, ^{2}H]-labeled protein in 5 % D_2O/95 % H_2O at pH 7.0. The lines represent the global fit to a two-state model using the Carver–Richards equation. The chemical shift differences $|\Delta\delta_{dia}|$ and $|\Delta\delta_{para}|$ obtained from the fit are provided in units of ppm. The globally optimized parameters k_{ex} and p_B are 678 s^{-1} and 0.2, respectively

basis of previously obtained assignments of w.t. ADK (Henzler-Wildman et al. 2007a). Assignments that unambiguously could be transferred from the spectrum of the w.t. protein to the spectrum of Lu-tagged ADK, and subsequently from the Lu-tagged to the Yb-tagged ADK spectrum, were used to obtain an initial susceptibility tensor and position of the Yb^{3+} ion. These initial parameters were used to predict the PCSs of the remaining residues, which then aided further assignment in an iterative manner, together with the tensor optimization (Schmitz et al. 2006). In this way, almost all observable signals in the ^{15}N HSQC spectra could be assigned. The agreement between observed and back-calculated PCSs based on the final tensor is shown in Fig. 1d. The agreement is good (Q = 0.068), except for a few residues mainly located in the mobile ATP lid (see Fig. 1a). This region is known to undergo large motions on the ps–ns time-scale (Henzler-Wildman et al. 2007b), thus extensive dynamic averaging of the PCSs is expected and the three conformers of the ATP lid observed in the crystal structure (Henzler-Wildman et al. 2007a) used for the PCS analysis may not be representative for the solution ensemble. Residues 127–144 in the ATP lid were, therefore, not used for the tensor optimization.

^{1}H CPMG dispersion measurements

^{1}H relaxation dispersion profiles of Yb(paramagnetic)- and Lu(diamagnetic)-labeled ADK were obtained at three temperatures (298, 308, and 318 K). For 121 residues relaxation dispersion profiles were obtained for both the Yb- and Lu-tagged protein at 308 K. A ^{1}H relaxation dispersion experiment (Orekhov et al. 2004) was used rather than the more conventional ^{15}N variant (Tollinger et al. 2001), because the gyromagnetic ratio of ^{1}H is ten times larger than that of ^{15}N. The PCSs of ^{15}N and ^{1}H amide nuclei are of similar size in units of ppm and, therefore, ten times smaller for ^{15}N in units of frequency. Consequently, the relaxation dispersion effect is up to a hundred times larger for ^{1}H than for ^{15}N in the fast-exchange regime, because then the effect is proportional to the square of $\Delta\omega$. In the intermediate regime the dispersion is roughly proportional to $\Delta\omega$, and only in the slow-exchange limit the effect is the same for ^{15}N and ^{1}H (Wang et al. 2007).

In Yb-tagged ADK ^{1}H relaxation dispersion is observed throughout the protein (Figs. 2, 3). In the corresponding diamagnetic Lu^{3+}-labeled protein only a few residues show significant relaxation dispersion, and the effect is overall much smaller. The dispersion in Yb-tagged ADK is

therefore primarily caused by fluctuations in the PCS, implying that the involved nuclei undergo substantial motions relative to the χ-tensor of the lanthanide.

Analysis of the CPMG dispersion profiles

The ^{1}H CPMG relaxation curves were first fitted individually using the Carver-Richards equation for two-site exchange (Eq. 4). Similar k_{ex} values, within the estimated errors, were obtained for most residues (Figure S2 and Table S1), suggesting that the relaxation dispersions all result from the same global exchange process that is described well by a two-site exchange.

The exchange rate, k_{ex}, and the population, p_B, were estimated from a global fit. The obtained k_{ex} values are 395 ± 40, 678 ± 33, and 1,291 ± 50 s^{-1} at 298, 308, and 318 K respectively (Figure S4). From these values an activation energy of 49 ± 4 kJ/mol is obtained using the Arrhenius equation. The obtained value of p_B of 0.2 is less precise, because most resonances are in fast exchange as explained in the "Experimental Section".

The nature of the conformational exchange

The paramagnetic relaxation dispersion data clearly show that the Ln-tagged ADK undergoes conformational exchange. ADK is known to be an intrinsically flexible molecule that undergoes large conformational changes even in the absence of substrates (Henzler-Wildman et al. 2007a), thus, it is tempting to attribute the observed dispersions to these well-established motions. However, several features of the dispersion data are not in line with this idea: (1) The exchange rate is about five times slower than that previously reported (Henzler-Wildman et al. 2007a) for the intrinsic catalytic motions of ADK; (2) Only moderate dispersions are observed in the flexible ATP lid of Yb-tagged ADK. Lid closure is predicted to result in large PCS changes in this region and, therefore, in extensive line broadening, much larger than in other regions of ADK; (3) Sizable dispersion is observed in regions of ADK that according to the available crystal structures (Henzler-Wildman et al. 2007a), are not expected to have PCS perturbations due to lid opening/closing; most notable is the region 90–110. This region shows very clear relaxation dispersion in Yb-tagged ADK and practically no dispersion in Lu-ADK (Fig. 2). The region is located relatively far (20–30 Å) from the lanthanide tag and, therefore, the movement of this region needs to be substantial to account for the relaxation dispersion, because of the r^{-3} dependence of the PCS (Eq. 1). Simulations suggest that at least a 10 Å displacement is required. Such motion seems unreasonable, as it would require a major rearrangement of the entire protein structure that would cause large dispersion also in the diamagnetic protein.

For all these reasons, the observed dispersion cannot solely be caused by internal dynamics of the protein itself. The effect must, at least in part, be caused by motions of the lanthanide tag. To determine whether the paramagnetic dispersion is only caused by tag motions or by a combined motion of the tag *and* the protein, a quantitative analysis of the PCS information was performed.

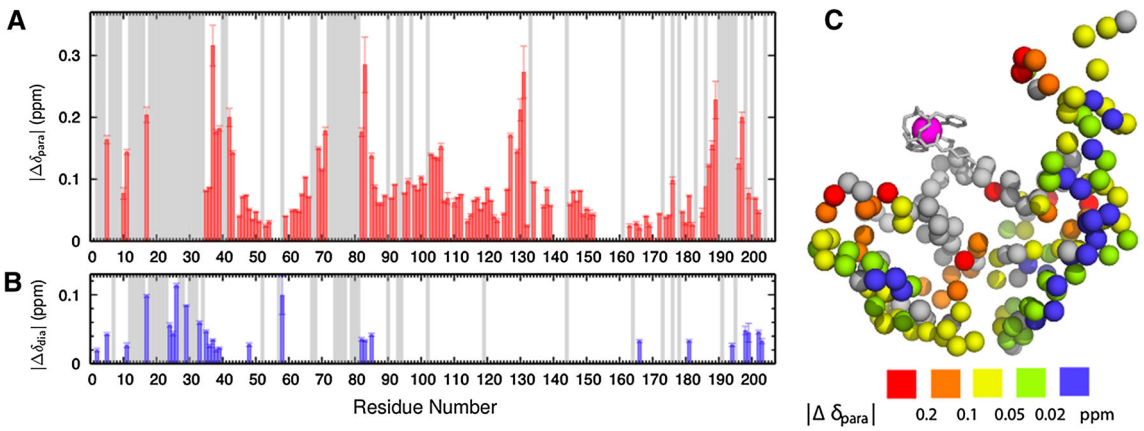

Fig. 3 **a**, **b** The frequency shifts |Δδ| between the major and minor form for Yb- and Lu-labeled ADK(K18C/K22C), respectively, obtained from the CPMG relaxation dispersion analysis. Here, the globally optimized exchange rate of 678 ± 33 s^{-1} and a population p_B of 0.2 was used, whereas R_2^0 and Δω, were fitted per residue using Eq. 4. *Error bars* show the estimated standard error (±1σ) obtained from the fits. *Grey areas mark* the residues for which no results were obtained. **c** The backbone amide protons (*small spheres*) in the structure of *A.a.* ADK are *colored* by the size of $|\Delta\delta_{para}|$ from *red* to *blue*, where *blue* corresponds to protons with no significant relaxation dispersion and protons for which no relaxation dispersion data were obtained are *colored gray*. The CLaNP-5 tag (*sticks*) with a Ln ion (*large magenta sphere*) was modeled on the structure

Determination of PCS of the minor state

Besides the rate and populations, the analysis of the CPMG dispersion profiles provides $|\Delta\omega|$ for the paramagnetically and the diamagnetically labeled protein (Fig. 3). In the paramagnetic case ΔPCS is encoded in $|\Delta\omega|$ (see "Theory" section). To determine ΔPCS, the sign of $\Delta\delta_{para}$ and $\Delta\delta_{dia}$ has to be known. Various techniques to obtain the sign of $\Delta\omega$ have been developed (Skrynnikov et al. 2002; Auer et al. 2009, 2010). One of them is to determine the small field dependence of the chemical shift (Vallurupalli et al. 2008a). For a paramagnetic molecule this approach is problematic, because also the paramagnetic alignment and, thereby, the ΔRACS contribution, is field dependent. Spinlock-based approaches provide an alternative (Auer et al. 2009), but here we utilize the predictable relation between the PCS and molecular structure in order to determine the signs in an iterative fashion.

$\Delta\delta_{dia}$ of one nucleus has no obvious correlation with that of other nuclei. Therefore, for a given set of N nuclei, which show dispersion, there are 2^N different sets of chemical shift values that produce the same set of dispersion curves for a diamagnetic protein. Also for $\Delta\delta_{para}$ there are in principle 2^N solutions and consequently up to 4^N solutions for the PCS of the minor state (Eqs. 7). However, the individual $\Delta\delta_{para}$ values are not independent of each other. All $\Delta\delta_{para}$ values are directly related to the χ-tensor provided that $\Delta\delta_{dia}$ is small. The system can be considered a molecule with two rigid domains that can orient in two different ways relative to each other. One domain contains a paramagnetic center and the other one is diamagnetic. The diamagnetic domain experiences paramagnetic relaxation dispersion when it moves relative to the paramagnetic domain. The set of PCSs of the two states (Eqs. 7) each have six degrees of freedom (three translational and three rotational) provided that $\Delta\chi_{ax}$ and $\Delta\chi_{rh}$ are known (Eq. 1). Therefore, if a few signs of ΔPCS are guessed correctly, the remaining signs can be determined iteratively by fitting three rotational and translational parameters for each state using Eq. 1. It is reasonable to assume that the ΔPCS values for a subset of nuclei close to each other in space have the same sign. This is especially likely to occur when the nuclei are far from the lanthanide. Under this assumption there exist only two solutions, rather than 2^N. These two solutions are not degenerate. One solution fits significantly better, as shown in Table 1 and Figure S3.

The values of $\Delta\chi_{ax}$ and $\Delta\chi_{rh}$ of both the minor and major state were fixed to the values obtained from the fit of the Δχ-tensor to the PCS directly observed in the spectrum, namely 8.2×10^{-32} m^3 and 2.3×10^{-32} m^3, respectively. Using relaxation dispersion derived PCS_B values from a small subset of six to eight residues close to each other, the initial orientation of the χ-tensor was estimated. The back-predicted PCS were used to determine the sign of ΔPCS and $\Delta\delta_{dia}$ of additional residues, allowing more PCS to be included in the fit. In this way all signs were determined iteratively with the χ-tensor of the minor state. Finally, the position of the Ln ion was optimized together with the χ-tensor orientation and all signs were reevaluated.

Also the $\Delta\chi_{ax}$ and $\Delta\chi_{rh}$ values were optimized for the both states in an eight-parameter fit (Table S3). The relatively small differences between the Δχ values of the minor and major states are likely not to be significant and can be due to the fact that the positioning the Ln ion and the simultaneous determination of $\Delta\chi_{ax}$ and $\Delta\chi_{rh}$ tend to correlate in a subtle non-linear way that is difficult to evaluate (Shishmarev and Otting 2013). The CLaNP-5(Yb) tag has been used in many studies, exhibiting very similar tensor values (Keizers et al. 2008; Xu et al. 2009; Dasgupta et al. 2011; Bertini et al. 2012; Hiruma et al. 2013; Guan et al. 2013; Camacho-Zarco et al. 2015), because the tensor properties are determined by the coordinating ligands and averaging is limited due to the two-armed attachment. Therefore, in the final fit, we chose to keep the $\Delta\chi_{ax}$ and $\Delta\chi_{rh}$ fixed to the values determined from the observed PCS as described above. The assumption that $\Delta\chi_{ax}$ and $\Delta\chi_{rh}$ remain constant is also physically meaningful for reasons discussed later.

As mentioned, two possible solutions can be obtained, depending on whether the initial subset of nuclei has positive or negative ΔPCS. When a different subset of nuclei is used to determine the initial χ-tensor, the exact same two solutions were obtained. One of these solutions results in a significantly better agreement between observed and back-calculated PCS (Table 1; Figure S3). This solution is shown in Fig. 4. In conclusion, there is a straightforward way to determine all signs iteratively,

Table 1 Changes in the Δχ-tensor orientations and Ln positions according to the two possible PCS solutions obtained from relaxation dispersion data corresponding to different initial signs of $\Delta\delta_{para}$ (see also Figure S3)

	Solution 1	Solution 2
$\Delta\theta_z$	23°	31°
$\Delta\theta_x$	7°	73°
$\Delta\theta_y$	24°	81°
Ln(A) − Ln(B)	0.6 ± 0.2 Å	3.3±1 Å
Ln(A) − C^α(C18/C22)	6.9/7.7 Å	7.0/8.0 Å
Ln(B) − C^α(C18/C22)	6.7/7.6 Å	6.1/5.5 Å
Q (A)	0.103	0.083
Q (B)	0.073	0.335

All values are derived from relaxation dispersion data recorded at 308 K. $\Delta\theta_z$, $\Delta\theta_x$, and $\Delta\theta_y$ are the differences in angle between the *z*-, *x*-, and *y*-axes, respectively, of the Δχ-tensors of the major and minor conformations A and B. All values are determined from a six parameter fit to Eq. 1 with $\Delta\chi_{ax} = 8.2\times10^{-32}$ m^3 and $\Delta\chi_{rh} = 2.3\times10^{-32}$ m^3

together with the structural parameters in the case where the motion can be described by a few degrees of freedom.

The results show that motion of the Ln tag can account for all the observed relaxation dispersion effects. The most pronounced difference between the minor and major state of the Ln tag is a 23° rotation of the *z*-axis around the *x*-axis of the χ-tensor (Fig. 4c; Table 1). In addition, the Ln position moves ~1 Å in a direction that is approximately perpendicular to the C^{α}–C^{α} bond vector between the two cysteines linked to the Ln tag, while the distance to the Cys C^{α} atoms stays approximately the same. The orientation of the *x*-axis remains largely unchanged. These findings show that the tag is undergoing a sideways tilting motion.

Direct observation of the PCS for the higher energy state

The temperature dependence of the exchange rate suggests that the exchange occurs in the slow-exchange regime for many residues at 278 K. Indeed, a second set of weak signals appears in the ^{15}N HSQC spectrum when the temperature is lowered below 283 K (Fig. 5a).

The direct determination of the PCSs allows comparison with those determined from the relaxation dispersion experiments. In all cases, the sign of the ΔPCS predicted from the dispersion data matches the observed one at 278 K. Also the magnitudes of the shifts are in good agreement, although the directly observed ΔPCS are on average 10 % larger than the relaxation dispersion derived values (Fig. 5b). The slope of the linear fit shown in Fig. 5b is 0.87 ± 0.02. A slope of one is only expected if the PCS is temperature independent and furthermore the p_B value (0.2) is correct. If the PCS is assumed to follow a Curie-like behavior (Bertini et al. 2002) the PCS is expected to be 10 % larger at 278 K than at 308 K, which accounts for the slope of 0.87 in Fig. 5b. The temperature dependence can also be determined experimentally by the slope of the linear fit to the CPMG derived PCS_A versus the

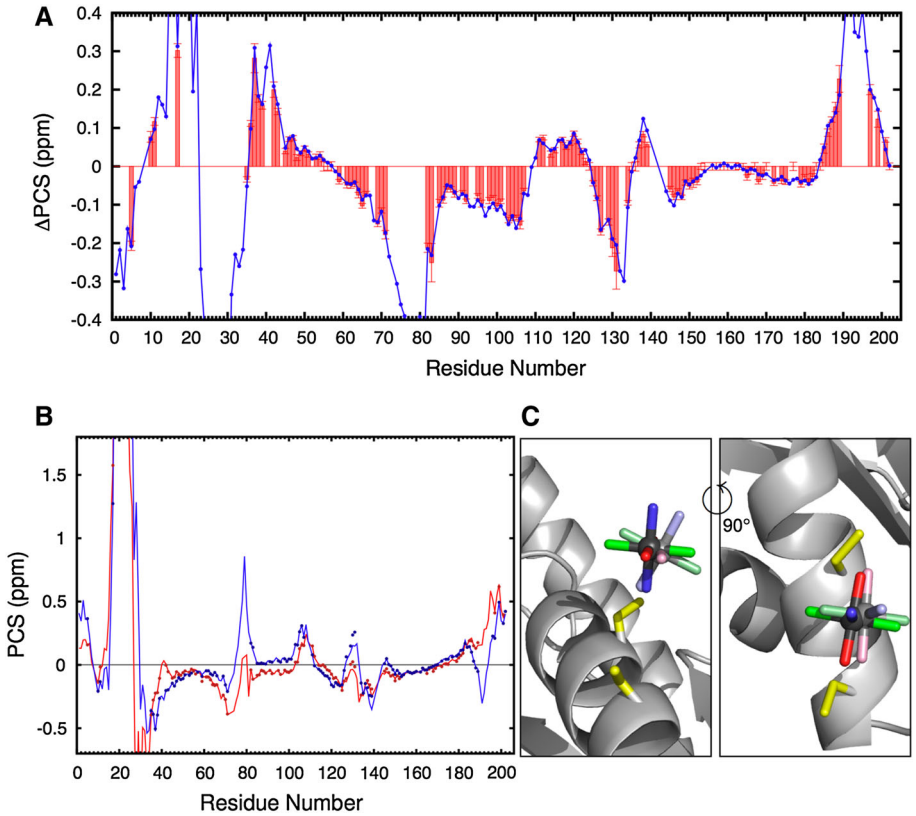

Fig. 4 CPMG dispersion reports on two Ln positions. **a** The ^{1}H PCS difference between the major and minor conformation of CLaNP-5 tagged ADK. *Red bars* represent the experimental ΔPCS derived from the CPMG measurements. The *blue line* represents the back-calculated values from the two tensors and the two Ln positions (**c**) determined from the experimental PCS of the major and minor form, shown in **b**. **b** The experimental (*dots*) and back-calculated (*lines*) PCS of the major (PCS_A, *blue*) and minor (PCS_B, *red*) conformation of the tag. **c** The χ-tensor frame and Ln position (*sticks*) seen from two different angles of the major (*dark colors*) and minor (*light colors*) conformation are shown together with the protein (*ribbon*). The *x*-, *y*-, and *z*-axes are *colored red*, *green*, and *blue*, respectively. The two views are rotated 90° relative to each other around the *y*-axis. Both tensor frames are associated with $\Delta\chi_{ax}$ and $\Delta\chi_{rh}$ values of 8.2×10^{-32} m^3 and 2.3×10^{-32} m^3, respectively. The *grey sphere* represents the Ln atom and the two Cys mutations of the tag attachment are shown with *yellow sticks*

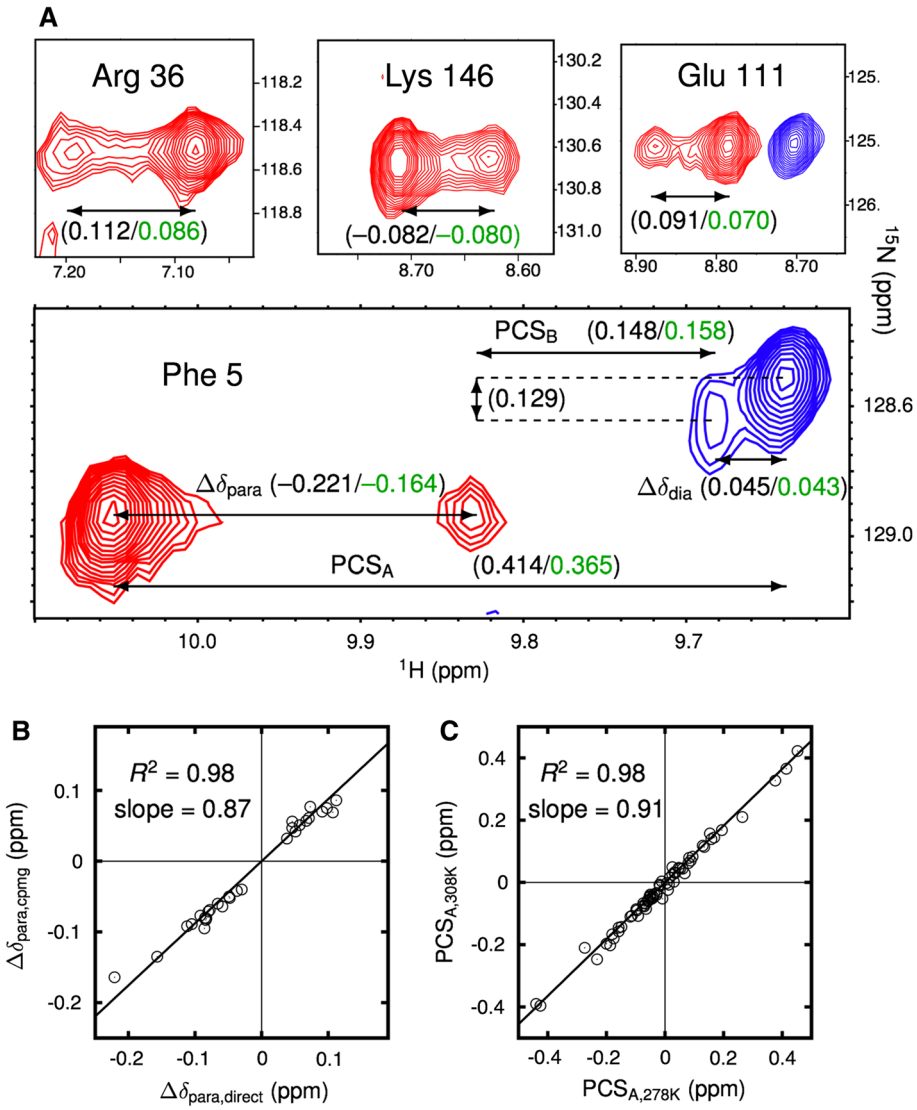

Fig. 5 Validation of the CPMG-derived PCS. **a** Examples of signals in the ^{15}N-TROSY spectrum at 278 K showing separate peaks for the major and minor orientation of the CLaNP-5 tag. Signals from Yb- and Lu-labeled ADK are *colored red* and *blue*, respectively. The *arrows highlight* the relevant shift differences and their values as measured in the spectrum (*black*) and as determined from CPMG relaxation dispersion measurements at 308 K (*green*), given in units of ppm. **b** The CPMG-derived $\Delta\delta_{para}$ values at 308 K versus the directly measured values at 278 K. **c** The PCS of the major orientation (PCS$_A$) obtained from measurements at 308 K and using Eqs. 7 versus the values measured directly at 278 K. The slope of the fitted *line* in **c** accounts for the overall temperatures dependence of the PCS

directly observed, which is 0.91 ± 0.01 (Fig. 5c). This measure is practically independent of p_B and reflects the average temperature dependence of the PCS. Corrections for this temperature dependence result in a p_B value of 0.18, in surprisingly good agreement with the value of 0.2 estimated from the dispersion measurements.

An example that illustrates the consistency between directly observed shifts and the CPMG dispersion data is the amide signal of Phe 5 in the ^{15}N-TROSY spectrum at 278 K (Fig. 5a), which features fast, intermediate, and slow exchange for different nuclei in the para- and diamagnetic proteins: In both the diamagnetic and paramagnetic spectrum the signals of the major and minor state are resolved, in agreement with the fact that both exhibit relaxation dispersion at higher temperature. At 308 K PCS$_{obs}$, which is the experimental PCS measured between the paramagnetic and the diamagnetic exchange-averaged peaks, is 0.324 ppm and the values of $|\Delta\delta_{para}|$ and $|\Delta\delta_{dia}|$, derived from the relaxation dispersion experiments, are 0.164 and 0.043 ppm, respectively. The back-calculated values from the $\Delta\chi$-tensor fit for PCS$_A$ and PCS$_B$ (the PCS values of the pure A and B state, respectively) are 0.365 and 0.158 ppm (Table S2). Entering these numbers in Eq. 7 with $p_B = 0.2$ shows that solution I is the correct solution for this residue. This solution corresponds to a negative $\Delta\delta_{para}$ value and a positive $\Delta\delta_{dia}$ value, which agrees with the observation at low temperatures (Fig. 5a). Furthermore, the fact that the diamagnetic signal is in slow exchange in the ^{1}H dimension at 278 K suggests that at this temperature k_{ex} is significantly lower than the rate at coalescence, $\Delta\omega/\sqrt{2} = 120\ s^{-1}$. In the ^{15}N dimension, the minor signal is shifted relative to the major state in the diamagnetic spectrum. Thus, the exchange is intermediate or slow in the diamagnetic protein, whereas in the

paramagnetic protein the ^{15}N nucleus is in fast exchange, since the minor and major peaks occur at the same frequency. Also, the minor signal appears sharper in the paramagnetic spectrum. Although it may seem counterintuitive that paramagnetism leads to line narrowing, such findings are not unexpected. The back-predicted ^{15}N PCS of the minor and major states is 0.20 and 0.35 ppm, respectively. Thus, $\Delta PCS = -0.15$ ppm. Because the ^{15}N value of $\Delta\delta_{dia}$ is opposite in sign to ΔPCS, the diamagnetic and paramagnetic contributions to ^{15}N Phe 5 partly cancel and reduce the exchange broadening. The broader appearance in the ^{15}N dimension of the minor Phe 5 signal in the diamagnetic protein confirms that the exchange is close to coalescence. From the observed ^{15}N shift $\Delta\delta_{dia}$ is about 0.13 ppm, which corresponds to a rate at coalescence >35 s^{-1}. Thus, k_{ex} is likely to be faster than 35 s^{-1}, yet slower than 120 s^{-1}, which is in accord with a rate of 84 s^{-1} extrapolated from the dispersion data at higher temperatures (Figure S4).

Movements in DOTA based Ln tags

The relaxation dispersion data show that the CLaNP-5-tag bound to ADK(K18C/K22C) undergoes a 23° tilting motion between two distinct orientations with populations of 0.8 and 0.2, respectively, and an exchange with a rate of 400 s^{-1} at 298 K. Structural heterogeneity has been a persistent problem in the design of Ln tags (Grey et al. 2003; Vlasie et al. 2007). From the current data, the underlying mechanism of the CLaNP-5 motion cannot be deduced, as long as high-resolution structures of the tag attached to the protein are not available. Attempts in our groups to obtain a crystal structure of the protein-attached CLaNP-5 tag have been unsuccessful so far (unpublished results). Most likely the motion involves the linkers by which the Ln-cage is attached to the protein backbone. If conformational changes occur within the linkers, it is likely that also the Ln cage reorients (Fig. 6a). A possibility is that the disulphide bridges assume different rotameric states. Rotamerization of disulphide bonds on the μs–ms time-scale has been observed in proteins (Grey et al. 2003). However, the linkers themselves may not be the direct cause to the conformation change. DOTA based Ln cages (like CLaNP-5) are known to undergo a combination of coordinated ring-flips and reorientations of their four chelating arms (Fig. 6b) (Aime et al. 1992). These movements result in a dynamic equilibrium between two enantiomer forms of the Ln cage (Natrajan et al. 2010). A previous study showed that the CLaNP-5 tag not attached to a protein and loaded with Eu^{3+}, undergoes enantiomerization with an exchange rate of 200 s^{-1} at 298 K (Hass et al. 2010). The mirror symmetry ensures that the χ-tensor and the populations are the same for both observed forms of CLaNP-5. Yet, when bound to a protein, the symmetry is broken and together the tag and the protein form a pair of diastereomers. As illustrated in Fig. 6b the orientation of the DOTA structure differs for these two diastereomers. This symmetry breach may skew the populations significantly, for instance by destabilizing one of the diastereomers, so they become similar to those observed here (0.8 and 0.2). Also the exchange rate may be affected by the symmetry breach. Hypothetically, if the transition state of this process remains unaffected, the exchange rate becomes 500 s^{-1}—comparable to the rate observed here. The degree of stabilization of one diastereomer relative to the other would in this scenario depend on the properties of the attachment site and the linkers. Both models in Fig. 6 account for the differences in dynamics reported for various attachments of the CLaNP-5 tag (Hass et al. 2010). In both cases the conformational change has little effect on the local environment of the Ln. Therefore it is reasonable to assume that $\Delta\chi_{ax}$ and $\Delta\chi_{rh}$ are the same for both the major and minor conformation.

Conclusions

The results show that CPMG relaxation dispersion in paramagnetic systems can be used to obtain accurate quantitative PCSs of higher energy conformations. The major advantages of CPMG dispersion with lanthanide tagged proteins are illustrated: (1) Detailed structural information about the higher energy state can be obtained and (2) larger dispersion amplitudes than observed for diamagnetic systems can be achieved.

Our results also point toward an inherent problem that yet needs to be solved, in order to observe PCS suitable for structure calculation of minor states. Even with a two-point attached probe like CLaNP-5, mobility on the μs–ms timescale can be a problem. In this study we show that a relatively modest 23° tilting motion of the tag results in dispersion effects throughout the protein. Two possible mechanisms for this motion are given. Either tag movement results from a conformational equilibrium of the linkers, e.g. between different rotamers of the disulphide bond, or the tag movement is caused by the enantiomerization of the Ln cage. Although tag motions observed here with relaxation dispersion have major implications for the observation of higher energy states of proteins, it should be emphasized that their impact on ground states studies remains minor. The fit of predicted vs. observed PCS to a single tensor is excellent and the size of the axial component of the $\Delta\chi$ is not reduced significantly, indicating that the PCS averaging effect over the two states is very small. The CLaNP tags have been successfully used to structurally characterize proteins and protein complexes, assuming

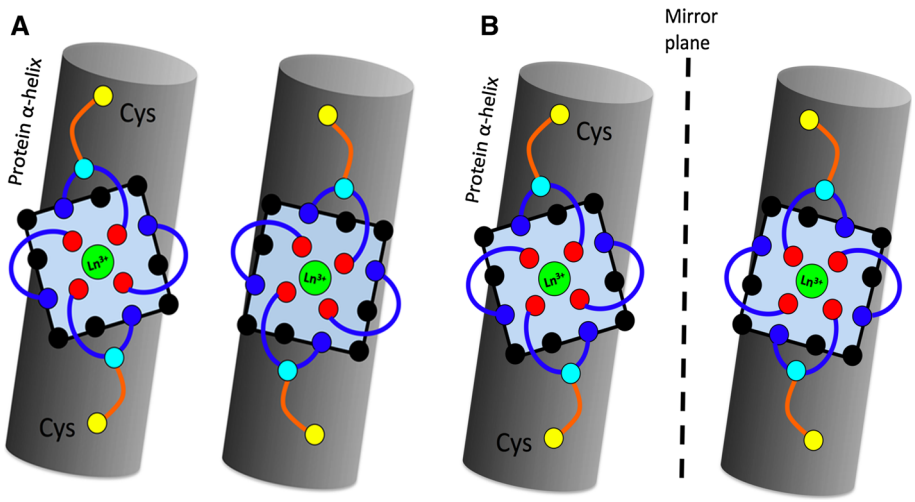

Fig. 6 A schematic representation of two hypothetical mechanisms for the motion of the CLaNP-5 tag attached to a protein. **a** A conformational change in the linkers reorients the Ln cage. **b** The protein attachment breaks the symmetry between the two enantiomers of the tag. Together, the tag and protein form two diastereomers, with different energies and different χ-tensor orientations. Lanthanide ion (*green dots*), carbon atoms in the cyclen ring (*black dots*), Ln-chelating oxygen atoms (*red dots*), Ln-chelating nitrogen atoms (*blue dots*), amide nitrogen (*cyan dots*), sulfur atom (*yellow dots*). Cyclen ring (*black lines*), chelating arms (*blue lines*), linkers (*orange lines*), protein helix (*grey cylinder*). The *dotted line* represents the (pseudo) mirror plane of the enantiomers of the tag

a single effective χ-tensor orientation (Keizers et al. 2007, 2008; Xu et al. 2009; Keizers et al. 2010; Dasgupta et al. 2011; Bertini et al. 2012; Liu et al. 2012; Hiruma et al. 2013).

The tag mobility observed in this study may be a property of the linkers. If this is the case, the problem may be solved by altering the mobility of the linkers, thereby moving the mobility of the tag out of the time window in which relaxation dispersion is sensitive. Probes attached via more flexible linkers may only exhibit dynamics on shorter time-scales. Such tags, however, often have ill-defined positions, leading to averaging effects that could complicate the interpretation of the minor state PCS in structural terms. More bulky tags may have limited mobility due to a large number of interactions with the protein (Koehler and Meiler 2011). Yet, large tags have the disadvantage that they may influence the intrinsic motions of the protein. If the tag mobility is caused by intrinsic motions of the Ln site, such as the enantiomerization of Ln cage, it may be a solution to use rigidified Ln cages, for example by methyl groups to the cyclen ring and/or the pendant arms (Haussinger et al. 2009). As we found cases in which the mobility of CLaNP-5 can be small enough to yield useful relaxation dispersion data on intrinsic protein motions (Hass et al. 2010), it may be possible to establish rules for probe attachment sites that define such low mobility locations on the protein surface. We further pursue these various possibilities, motivated by the great potential of paramagnetic relaxation dispersion for structural characterization of lowly populated states.

Electronic supporting material

Figures showing the quality of the global fit of the dispersion profiles as a function of p_B; k_{ex} determined from a per residue fit of the CPMG dispersion data; the two different PCS solutions corresponding to different signs of ΔPCS; k_{ex} versus temperature; tables with the parameters k_{ex}, omega, R_2^0 fitted for each dispersion profile of each individual residue; results from the global fit of the CPMG dispersion data, the derived PCS values, and PCS_{obs}; results from the eight parameter fit of the Δχ-tensor and the Ln position of the minor and major conformation.

Acknowledgments Financial support was provided by the Netherlands Organisation for Scientific Research grants 700.10.407 (M.A.S.H) and 700.58.441 (M.U., W.M.L. and J.T.S.), the Howard Hughes Medical Institute and the Office of Basic Energy Sciences, Catalysis Science Program, U.S. Dept. of Energy, award DE-FG02-05ER15699 and National Institutes of Health, award GM100966-01 (R.V.A., L.A.P., R.O. and D.K.), and R.O. is a HHMI Fellow of the Damon Runyon Cancer Research Foundation, DRG-2114-12.

Conflict of interest The authors declare that they have no conflict of interest.

References

Aime S, Botta M, Ermondi G (1992) NMR study of solution structures and dynamics of lanthanide(III) complexes of DOTA. Inorg Chem 31:4291–4299

Auer R, Neudecker P, Muhandiram D, Lundstrom P, Hansen D, Konrat R, Kay LE (2009) Measuring the signs of ^{1}Hα chemical shift differences between ground and excited protein states by

off-resonance spin-lock $R_{1\rho}$ NMR spectroscopy. J Am Chem Soc 131:10832–10833

Auer R, Hansen D, Neudecker P, Korzhnev DM, Muhandiram D, Konrat R, Kay LE (2010) Measurement of signs of chemical shift differences between ground and excited protein states: a comparison between H(S/M)QC and $R_{1\rho}$ methods. J Biomol NMR 46:205–216

Bertini I, Luchinat C, Parigi G (2002) Magnetic susceptibility in paramagnetic NMR. Progr Nucl Magn Reson Spect 40:249–273

Bertini I, Calderone V, Cerofolini L, Fragai M, Geraldes CFGC, Hermann P, Luchinat C, Parigi G, Teixeira JMC (2012) The catalytic domain of MMP-1 studied through tagged lanthanides. FEBS Lett 586:557–567

Bouvignies G, Markwick P, Bruscheweiler R, Blackledge M (2006) Simultaneous determination of protein backbone structure and dynamics from residual dipolar couplings. J Am Chem Soc 128:15100–15101

Bouvignies G, Vallurupalli P, Hansen DF, Correia BE, Lange O, Bah A, Vernon RM, Dahlquist FW, Baker D, Kay LE (2011) Solution structure of a minor and transiently formed state of a T4 lysozyme mutant. Nature 477:111–114

Camacho-Zarco AR, Munari F, Wegstroth M, Liu WM, Ubbink M, Becker S, Zweckstetter M (2015) Multiple paramagnetic effects through a tagged reporter protein. Angew Chem Int Ed 54:336–339

Carver JP, Richards RE (1972) A general two-site solution for the chemical exchange produced dependence of T_2 upon the Carr-Purcell pulse separation. J Magn Reson 6:89–105

Cornilescu G, Marquardt JL, Ottiger M, Bax A (1998) Validation of protein structure from anisotropic carbonyl chemical shifts in a dilute liquid crystalline phase. J Am Chem Soc 120:6836–6837

Dasgupta S, Hu XY, Keizers PHJ, Liu WM, Luchinat C, Nagulapalli M, Overhand M, Parigi G, Sgheri L, Ubbink M (2011) Narrowing the conformational space sampled by two-domain proteins with paramagnetic probes in both domains. J Biomol NMR 51:253–263

Delaglio F, Grzesiek S, Vuister GW, Zhu G, Pfeifer J, Bax A (1995) NMRPipe—A multidimensional spectral processing systeme based on UNIX pipes. J Biomol NMR 6:277–293

Eichmueller C, Skrynnikov NR (2007) Observation of μs time-scale protein dynamics in the presence of Ln(3+) ions: application to the N-terminal domain of cardiac troponin C. J Biomol NMR 37:79–95

Grey MJ, Wang CY, Palmer AG (2003) Disulfide bond isomerization in basic pancreatic trypsin inhibitor: multisite chemical exchange quantified by CPMG relaxation dispersion and chemical shift modeling. J Am Chem Soc 125:14324–14335

Guan JY, Keizers PHJ, Liu WM, Lohr F, Skinner SP, Heeneman EA, Schwalbe H, Ubbink M, Siegal G (2013) Small-molecule binding sites on proteins established by paramagnetic NMR spectroscopy. J Am Chem Soc 135:5859–5868

Hass MAS, Keizers PHJ, Blok A, Hiruma Y, Ubbink M (2010) Validation of a lanthanide tag for the analysis of protein dynamics by paramagnetic NMR spectroscopy. J Am Chem Soc 132:9952–9953

Haussinger D, Huang JR, Grzesiek S (2009) DOTA-M8: an extremely rigid, high-affinity lanthanide chelating tag for PCS NMR spectroscopy. J Am Chem Soc 131:14761–14767

Henzler-Wildman KA, Thai V, Lei M, Ott M, Wolf-Watz M, Fenn T, Pozharski E, Wilson MA, Petsko GA, Karplus M, Hubner CG, Kern D (2007a) Intrinsic motions along an enzymatic reaction trajectory. Nature 450:838–844

Henzler-Wildman KA, Lei M, Thai V, Kerns SJ, Karplus M, Kern D (2007b) A hierarchy of timescales in protein dynamics is linked to enzyme catalysis. Nature 450:913–916

Hiruma Y, Hass MAS, Kikui Y, Liu WM, Olmez B, Skinner SP, Blok A, Kloosterman A, Koteishi H, Lohr F, Schwalbe H, Nojiri M, Ubbink M (2013) The structure of the cytochrome P450cam-putidaredoxin complex determined by paramagnetic NMR spectroscopy and crystallography. J Mol Biol 425:4353–4365

John M, Park AY, Pintacuda G, Dixon NE, Otting G (2005) Weak alignment of paramagnetic proteins warrants correction for residual CSA effects in measurements of pseudocontact shifts. J Am Chem Soc 127:17190–17191

Keizers PHJ, Ubbink M (2011) Paramagnetic tagging for protein structure and dynamics analysis. Progr Nucl Magn Reson Spect 58:88–96

Keizers PHJ, Desreux JF, Overhand M, Ubbink M (2007) Increased paramagnetic effect of a lanthanide protein probe by two-point attachment. J Am Chem Soc 129:9292–9293

Keizers PHJ, Saragliadis A, Hiruma Y, Overhand M, Ubbink M (2008) Design, synthesis, and evaluation of a lanthanide chelating protein probe: CLaNP-5 yields predictable paramagnetic effects independent of environment. J Am Chem Soc 130:14802–14812

Keizers PHJ, Mersinli B, Reinle W, Donauer J, Hiruma Y, Hannemann F, Overhand M, Bernhardt R, Ubbink M (2010) A solution model of the complex formed by adrenodoxin and adrenodoxin reductase determined by paramagnetic NMR spectroscopy. Biochemistry 49:6846–6855

Koehler J, Meiler J (2011) Expanding the utility of NMR restraints with paramagnetic compounds: background and practical aspects. Progr Nucl Magn Reson Spect 59:360–389

Liu WM, Keizers PHJ, Hass MAS, Blok A, Timmer M, Sarris AJC, Overhand M, Ubbink M (2012) A pH-sensitive, colorful, lanthanide-chelating paramagnetic NMR probe. J Am Chem Soc 134:17306–17313

Markwick PR, Bouvignies G, Salmon L, McCammon J, Nilges M, Blackledge M (2009) Toward a unified representation of protein structural dynamics in solution. J Am Chem Soc 131:16968–16975

Monod J, Wyman J, Changeux JP (1965) On the nature of allosteric transitions: a plausible model. J Mol Biol 12:88–118

Natrajan LS, Khoabane NM, Dadds BL, Muryn CA, Pritchard RG, Heath SL, Kenwright AM, Kuprov I, Faulkner S (2010) Probing the structure, conformation, and stereochemical exchange in a family of lanthanide complexes derived from tetrapyridyl-appended cyclen. Inorg Chem 49:7700–7709

Orekhov VY, Korzhnev DM, Kay LE (2004) Double- and zero-quantum NMR relaxation dispersion experiments sampling millisecond time scale dynamics in proteins. J Am Chem Soc 126:1886–1891

Otting G (2008) Prospects for lanthanides in structural biology by NMR. J Biomol NMR 42:1–9

Palmer AG, Kroenke CD, Loria JP (2001) Nuclear magnetic resonance methods for quantifying microsecond-to-millisecond motions in biological macromolecules. Methods Enzymol 339:204–238

Pervushin K, Riek R, Wider G, Wuthrich K (1997) Attenuated T_2 relaxation by mutual cancellation of dipole-dipole coupling and chemical shift anisotropy indicates an avenue to NMR structures of very large biological macromolecules in solution. Proc Natl Acad Sci USA 94:12366–12371

Schmitz C, John M, Park AY, Dixon NE, Otting G, Pintacuda G, Huber T (2006) Efficient Chi-tensor determination and NH assignment of paramagnetic proteins. J Biomol NMR 35:79–87

Schmitz C, Stanton-Cook MJ, Su XC, Otting G, Huber T (2008) Numbat: an interactive software tool for fitting Delta Chi-tensors to molecular coordinates using pseudocontact shifts. J Biomol NMR 41:179–189

Shishmarev D, Otting G (2013) How reliable are pseudocontact shifts induced in proteins and ligands by mobile paramagnetic metal tags? A modelling study. J Biomol NMR 56:203–216

Skrynnikov NR, Dahlquist FW, Kay LE (2002) Reconstructing NMR spectra of "invisible" excited protein states using HSQC and HMQC experiments. J Am Chem Soc 124:12352–12360

Tollinger M, Skrynnikov NR, Mulder FAA, Forman-Kay JD, Kay LE (2001) Slow dynamics in folded and unfolded states of an SH3 domain. J Am Chem Soc 123:11341–11352

Torda AE, Scheek RM, van Gunsteren WF (1990) Time-averaged nuclear Overhauser effect distance restraints applied to tendamistat. J Mol Biol 214:223–235

Vallurupalli P, Hansen DF, Stollar E, Meirovitch E, Kay LE (2007) Measurement of bond vector orientations in invisible excited states of proteins. Proc Natl Acad Sci USA 104:18473–18477

Vallurupalli P, Hansen DF, Kay LE (2008a) Probing structure in invisible protein states with anisotropic NMR chemical shifts. J Am Chem Soc 130:2734–2735

Vallurupalli P, Hansen DF, Kay LE (2008b) Structures of invisible, excited protein states by relaxation dispersion NMR spectroscopy. Proc Natl Acad Sci USA 105:11766–11771

Vlasie MD, Comuzzi C, Van den Nieuwendijk AMCH, Prudencio M, Overhand M, Ubbink M (2007) Long-range-distance NMR effects in a protein labeled with a lanthanide-DOTA chelate. Chem Eur J 13:1715–1723

Vranken WF, Boucher W, Stevens TJ, Fogh RH, Pajon A, Llinas P, Ulrich EL, Markley JL, Ionides J, Laue ED (2005) The CCPN data model for NMR spectroscopy: development of a software pipeline. Prot Struct Funct Bioinform 59:687–696

Wang X, Srisailam S, Yee AA, Lemak A, Arrowsmith C, Prestegard JH, Tian F (2007) Domain-domain motions in proteins from time-modulated pseudocontact shifts. J Biomol NMR 39:53–61

Wolf-Watz M, Thai V, Henzler-Wildman K, Hadjipavlou G, Eisenmesser EZ, Kern D (2004) Linkage between dynamics and catalysis in a thermophilic-mesophilic enzyme pair. Nat Struct Mol Biol 11:945–949

Xu XF, Keizers PHJ, Reinle W, Hannemann F, Bernhardt R, Ubbink M (2009) Intermolecular dynamics studied by paramagnetic tagging. J Biomol NMR 43:247–254